A Numerical Model for Electromagnetic Scattering from Sea Ice

Elias M. Nassar, Joel T. Johnson, *Member, IEEE,* and Robert Lee

***Abstract*—A numerical model for scattering from sea ice based on the finite difference time domain (FDTD) technique is presented. The sea ice medium is modeled as consisting of randomly located spherical brine scatterers with a specified fractional volume, and the medium is modeled both with and without a randomly rough boundary to study the relative effects of volume and surface scattering. A Monte Carlo simulation is used to obtain numerical results for incoherent vv backscattered normalized radar cross sections (RCS's) in the frequency range from 3 to 9 GHz and for incidence angles from 10° to 50° from normal incidence. The computational intensity of the study necessitates an effective permittivity approach to modeling brine pocket effects and a nonuniform grid for small scale surface roughness. However, comparisons with analytical models show that these approximations should introduce errors no larger than approximately 3 dB. Incoherent vv cross sections backscattered from sea ice models with a smooth surface show only a small dependence on incidence angle, while results for sea ice models with slightly rough surfaces are found to be dominated by surface scattering at incidence angles less than 30° and by scattering from brine pockets at angles greater than 30°. As the surface roughness increases, surface scattering tends to dominate at all incidence angles. Initial comparisons with measurements taken with artificially grown sea ice are made, and even the simplified sea ice model used in the FDTD simulation is found to provide reasonable agreement with measured data trends. The numerical model developed can be useful in interpreting measurements when parameters such as surface roughness and scatterer distributions lie outside ranges where analytical models are valid.**

***Index Terms*—Remote sensing, rough surfaces, scattering, sea ice.**

I. Introduction

KNOWLEDGE of the depth, structure, and extent of sea ice cover in polar regions is important for the purpose of predicting global climate change and providing navigation information for marine vessels. Due to the difficulty in accessing polar regions, microwave remote sensing devices on orbiting satellites can be used to obtain information about sea ice cover. Measurements and scattering models are necessary for developing inverse models that can be used to extract sea ice physical parameters from the data obtained with the remote sensors. Physically-based scattering models necessarily contain both an electromagnetic component and an idealized representation of the complicated geometric arrangement of ice, brine, and air pockets in sea ice.

Both analytical and numerical models have been developed in the past for predicting backscattering from sea ice-like media. Analytical models can be divided in two major categories [1]: those that treat volume scattering and those that deal with rough surface scattering. Volume scattering models are primarily developed using either the radiative transfer theory (RTT) or analytic wave theory [2], [3], while surface scattering models make use of physical optics theory (PO) [4], the small perturbation method (SPM) [5], the integral equation method (IEM) [6] and other analytical techniques. In these analytical models, both for volume and surface scattering, electromagnetic approximations are needed in order to obtain a solution for the complicated analytical expressions that often result, even with a simplified description of the sea ice medium. In particular, when both volume and surface scattering are considered simultaneously, the resulting complexity of the formulation has caused only limited results to be obtained, and several questions remain regarding the relative importance of volume and surface scattering.

These issues motivate the use of numerical techniques for the electromagnetic solution. With numerical models, once the geometry of the problem is defined, the solution obtained contains all scattering terms predicted by Maxwell's equations and avoids the limitations of electromagnetic approximations made in the analytical methods. In addition, both volume and surface scattering can be considered simultaneously without additional approximation. However, the greatly increased computational requirements of numerical models have previously limited their application to studies of sea ice scattering. Recent increases in computer speed and memory and in scattering algorithm efficiency are now producing an increased interest in numerical modeling of geophysical media such as the ocean, land, or vegetation [7]–[10]. This paper continues these developments to investigate numerical models for scattering from sea ice.

In Section II of this paper, the three-dimensional (3-D) finite difference time domain (FDTD) model is presented and in Section III, several results for the backscattered radar cross section (RCS) from smooth and slightly rough surface sea ice are shown. Comparisons of FDTD data with measurements of the backscattered RCS from artificially grown sea ice taken at the Cold Regions Research and Engineering Laboratory (CRREL), Hanover, NH, are discussed in Section IV.

Manuscript received January 27, 1998; revised October 2, 1998. This work was supported in part by the Phillips Laboratory, Air Force Material Command, under Cooperative Agreement F29601-93-2-0001. These opinions, interpretations, conclusions, and recommendations are those of the authors and are not necessarily endorsed by the United States Air Force, Phillips Laboratory, or the U.S. Government.

E. M. Nassar is with the Department of Electrical and Computer Engineering, Notre Dame University, Zouk Mosbeh, Lebanon.

J. T. Johnson and R. Lee are with the Department of Electrical Engineering and ElectroScience Laboratory, The Ohio State University, Columbus, OH 43212 USA (johnson@ee.eng.ohio-state.edu).

Publisher Item Identifier S 0196-2892(00)00004-8.

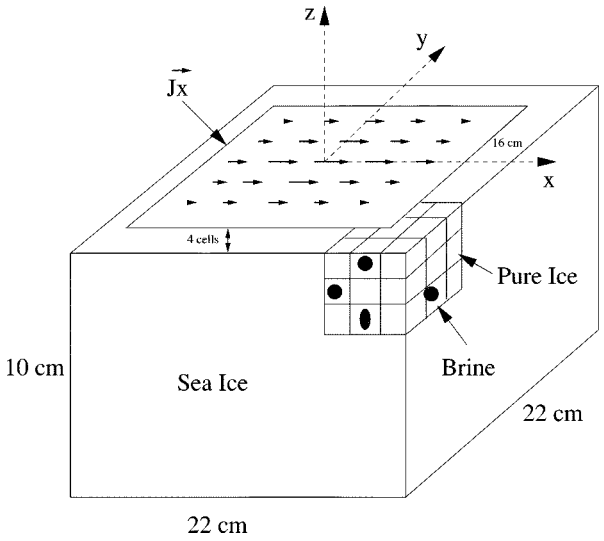

Fig. 1. FDTD model of sea ice showing the source location, brine pockets, and FDTD cells.

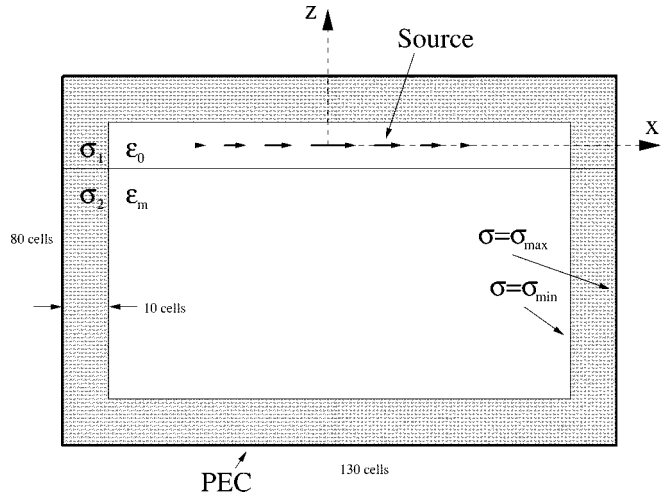

Fig. 2. Vertical cross section of FDTD domain.

II. FDTD Model for Sea Ice Scattering

Several numerical techniques could potentially be applied to investigate electromagnetic scattering from sea ice. However, in cases where results are desired over a wide range of frequencies, time domain methods offer distinct advantages. The FDTD technique [11] is currently the most widely used time domain method, and has been applied previously in studies of scattering from rough surfaces [8], [10], [12] and from objects in a material half space [13], [14]. The basic formulation of FDTD has been discussed extensively in the literature [15], and so is not repeated here. However, several issues arise when applying FDTD to scattering from an area extensive medium such as sea ice. The computational intensity of a three dimensional FDTD model will require some approximations in its implementation to remain numerically feasible; although these approximations will result in some loss of accuracy in absolute cross sections, conclusions regarding the relative influence of surface and volume scattering are expected to be relatively unaffected, so that valid insights into sea ice scattering should still be obtained. The following sections describe specific issues: generation of the incident field, the absorbing boundary condition, calculation of cross sections, Monte Carlo simulations, and modeling of sea ice structure.

A. Incident Field

Since plane waves represent a fundamental decomposition of any incident field, and since most previous sea ice scattering models have considered plane wave incidence, simulating an incident plane wave in the FDTD model would be desirable. However, developing source current densities in the FDTD that produce plane wave incident fields both above and below a dispersive half space is difficult and requires careful consideration [13]. The computational domain absorbing boundary conditions, described below, further exacerbate this problem, so an alternative approach was pursued using a finite source located inside the FDTD domain.

An impressed current density arranged in a square array as shown in Figs. 1 and 2 is used as the source of the incident field. For the case of normal incidence, current elements are in phase and for oblique incidence, the current elements have a time delay relative to each other that determines the incidence angle of the wave. Use of a finite source results in an incident "beam" on the sea ice medium, whose angular width is a frequency dependent quantity determined by the size of the antenna relative to the electromagnetic wavelength. Thus, scattered cross sections that are eventually obtained are averaged over this antenna pattern, resulting in a "smoothing" of the final results. Use of the beam has the desirable effect of reducing edge effects when computing scattered fields from the finite size FDTD domain, similar to the "tapered" incident field used in rough surface scattering studies [8]. However, care must be exercised in interpreting results if the source does not have a reasonable extent in terms of the electromagnetic wavelength at a given frequency.

The time domain source pulse is a differentiated Gaussian given by

$$J_x^n = \frac{(n\Delta t - AT)}{T^2} e^{-(n\Delta t - AT/T)^2} \tag{1}$$

where $A = 3.0$, $T = .1/2cA$, c is the speed of light in free space, and Δt is the time step. These constants are chosen to ensure that the incident pulse has most of its energy in the frequency range from 1 to 9 GHz. In order to reduce the sidelobe level of the incident beam, a spatially tapered current distribution is used for the source

$$J_x^n(x,y) = J_0 e^{(-(x^2+y^2)/C^2)} \tag{2}$$

where the constant C determines the taper of the incident beam.

Computational resources limit the meshed domain size to 130 $\times$ 130 $\times$ 80 cells. The space cell size Δx is chosen as 0.002 m, which is 1/16th of a free space wavelength at 9 GHz. The time step Δt is 3.0 ps. These dimensions (neglecting the PML regions) give a sea ice sample of $110 * .002 = 0.22$ m on a side and $50 * .002 = 0.1$ m high. The source is located at cell 65 in the z-direction and extends from cell 26 to cell 106 in the x and y-directions. The source array width is 0.16 m on a side, ranging

from 0.533λ at 1 GHz to 4.8λ at 9 GHz, and the taper width C is chosen to be 6 cm (producing a 12 cm diameter circular current at the e^{-1} points). Clearly, lower frequency results from the model will have a large degree of angular averaging. For this reason, only results from 3 GHz and above will be presented. In addition, use of a finite source inside the FDTD domain makes obtaining scattering predictions at 0° incidence difficult since specularly reflected results are very sensitive to the antenna pattern. Results at 0° will therefore not be presented. Use of the finite source will be validated in Section III through comparison with plane wave incidence SPM predictions for scattering from a slightly rough surface.

B. Absorbing Boundary Condition

The FDTD method requires an absorbing boundary condition to terminate the computational domain. The perfectly matched layer (PML) ABC [16], [17], which has been shown to provide excellent absorption characteristics for a wide range of incidence angles, is used for this purpose. Use of the PML ABC in a problem involving a half space requires the PML layer adjacent to the lower region to have the permittivity of the lower region. Therefore, the conductivity profile in PML is scaled according to whether the PML is adjacent to free space or the material [18]. The PML layer has a dielectric constant $\epsilon = \epsilon_m$ (that of the material adjacent to the PML) and a conductivity with a parabolic profile that increases from $\sigma_{\min}$ at the PML interface to $\sigma_{\max}$ at the PEC wall that terminates the PML. In this case, $\sigma_{\max} = 2.5$ Mho/m for the PML layer adjacent to the free space region and $W = 10 \times \Delta x = 0.02$ m (width of the PML layer). The PML is placed five cells away from the source in the z-direction and ten cells away in the x and y-directions. These choices for the PML parameters and location were found in several tests to provide adequate absorption [19]. Note that the finite source inside the domain radiates half of its energy upward toward the PML layer. However, no significant reflections of this energy were observed.

Scattered fields in the far-field region are found by first obtaining the total time domain field over a surface halfway between the source and the material interface, then Fourier transforming and using the surface equivalence principle to compute the equivalent surface electric and magnetic currents which, when integrated, give the far field values in the frequency domain. An initial validation of the FDTD model was done by comparison with two cases where an analytical solution was available: radiation from a finite source in free space and scattering from an infinite PEC plane illuminated by a finite source. In both cases, very good agreement was obtained between the FDTD and analytical results in the far field [19]–[20].

C. Bistatic RCS

Simulation results will be presented in terms of backscattered normalized radar cross sections. For an area-extensive target, the normalized RCS is defined as

$$\sigma^0_{\alpha,\beta}(\theta_s,\phi_s,\theta_i,\phi_i) = \lim_{R\to\infty} 4\pi R^2 \frac{S^s_\alpha(\theta_s,\phi_s)}{A_i S^i_\beta(\theta_i,\phi_i)} = \lim_{R\to\infty} 4\pi R^2 \frac{S^s_\alpha(\theta_s,\phi_s)\cos(\theta_i)}{P^i_\beta(\theta_i,\phi_i)} \quad (3)$$

where A_i is the area illuminated by the incident beam that coincides with the cross section of the computational domain excluding the PML region. S^s_α is the amplitude of the scattered Poynting vector in polarization α, P^i_β is the incident power in polarization β, and α, β indicates the polarization of the scattered and incident waves respectively (i.e., vv, vh, hv, and hh). For the FDTD model, the power incident on the surface of the sea ice sample is given by

$$P^i = \tfrac{1}{2}\ \mathrm{Re} \int_{x1}^{x2}\int_{y1}^{y2} \hat{z}\cdot\overline{E}^i \times \overline{H}^{i*}\, dx\, dy \quad (4)$$

where $x1$, $x2$, $y1$, and $y2$ are the limits of the area A_i mentioned above and located in a horizontal plane four cells away from the source in the vertical direction. To obtain the incident power on the surface of the material being modeled, the FDTD code is run for the case of the source in free space and the above integral is computed at each frequency. Only vv-polarized cross sections are considered in this study due to computational limitations and the very small values of hv cross sections obtained, which are more susceptible to numerical errors.

D. Monte Carlo Simulations

Since the location of brine pockets in sea ice and the surface roughness profile are random, statistical properties of scattered cross sections will be described by averaging FDTD frequency domain fields obtained from several realizations of the sea ice medium. Both coherent and incoherent averages can be computed. Coherent averages are expressed as

$$S_{coh} \propto |\langle E_n\rangle|^2 \quad (5)$$

where the symbol $\langle\ \rangle$ indicates an average over all the realizations, and E_n is the scattered electric field for realization n. The incoherent power is given by

$$S_{inc} \propto \langle |E_c - E_n|^2\rangle \quad (6)$$

where E_c is the coherent electric field. Expressions for the coherent and incoherent RCS use either S_{coh} or S_{inc} for S^s in (3), respectively. Only incoherent results will be illustrated. Coherent backscattered cross sections primarily exist at 0° incidence and are not plotted for the reasons discussed earlier.

Monte Carlo simulations were performed using the IBM SP/2 parallel supercomputer at the Maui High Performance Computing Center (MHPCC), Maui, HI. The IBM SP/2 is a collection of 400 RS-6000 workstation nodes, roughly of typical PENTIUM II performance individually, networked through a high performance communication system to allow groups of nodes to operate in combination as a parallel processor. Since each realization is independent of all others in a Monte Carlo simulation, FDTD calculations for each realization were performed on individual nodes of the IBM SP/2 with only minimal communications required. Backscattered cross sections were computed at incidence angles from 10° to 50° in 10° increments, requiring five separate Monte Carlo runs. Convergence tests in the Monte Carlo simulation showed that eight realizations were sufficient to provide convergence of averaged incoherent backscattered cross sections to within 3 dB. Although a larger number of realizations to obtain more accuracy would be desirable, computational limitations prohibited additional studies. Thus, for each physical configuration of the sea ice medium (fractional volume

or surface parameters), 40 FDTD runs were performed in parallel on 40 SP/2 nodes. Execution time for each run is 3 h on an SP2 node of the MHPCC, and the required memory storage is 114 Mb. Computation of the coherent and incoherent fields is done in a postprocessing step after all the results are obtained from the MHPCC.

E. Generation of Random Distribution of Scatterers

A final issue involves the model used for the sea ice medium. The extremely small size of typical brine pockets (0.75 mm or smaller) in sea ice makes discretizing individual brine pocket structures impossible given computational limitations. To avoid this problem, an effective permittivity approach is used. A uniform $(0,1)$ random number generator is first used to determine the presence or absence of a single brine pocket in each 2 mm cubic cell of the FDTD mesh. Although this procedure implies a nonuniform pair distribution function, the obtained distribution of brine pockets should be approximately uniform for low to moderate brine fractional volumes. The threshold for the random number generator is determined by the fractional volume of brine in the sea ice sample as follows. Given the fractional volume of brine f_b and the size of the brine pocket v_b, we can determine the number n_b of brine pockets in the sea ice sample

$$n_b = \frac{V f_b}{v_b} \tag{7}$$

where V is the volume of the FDTD domain excluding the PML region. If the number of FDTD cells is N, the random number generator threshold t is (given the presence of one brine pocket per FDTD cell)

$$t = \frac{n_b}{N}. \tag{8}$$

Since the volume of the brine inclusion is smaller than that of the FDTD cell, the fractional volume of the FDTD cells that contain brine inclusions (f_{FDTD}) is related to that of the brine inclusions (f_b) by

$$f_{FDTD} = f_b \frac{v_{FDTD}}{v_b} \tag{9}$$

where v_b and v_{FDTD} are the volumes of the brine inclusion and the FDTD cell, respectively.

The effective permittivity approach is applied in determining the effective dielectric constant of an FDTD cell, which is partially filled with a brine pocket. For this purpose, standard mixing laws are applied [21] for a sphere embedded in a background medium, resulting in a permittivity of the FDTD cell that is less than that of brine. Thus, the resulting medium contains a large fractional volume of low permittivity scatterers intended to model a medium with a smaller fractional volume of higher permittivity scatterers. This procedure is justified due to the small size of the brine scatterers compared to the electromagnetic wavelength, for which the use of mixing laws should be valid. Tests comparing predictions of first-order radiative transfer theory [22] for the true brine scatterers and the FDTD approximated scatterers showed cross sections within 2 dB, and comparisons with a first-order radiative transfer solution in the next section will also provide some validation for this approach. Results in the next section comparing the relative influence of surface and volume scattering also should be relatively unaffected by errors introduced in the effective permittivity method.

Since the FDTD method is a time domain method, variations in medium permittivity with frequency are difficult to model and require special methods that further increase computational requirements and were therefore not possible. An additional approximation assumed scatterer permittivities to have a constant real part versus frequency and an imaginary part determined through an effective conductivity defined at the center frequency of interest. Note that this definition is made after the application of the mixing law, so FDTD cell permittivity variations versus frequency are significantly smaller than those of brine alone.

III. Numerical and Analytical Solutions for Sea Ice Scattering

Results from the Monte Carlo simulations are illustrated for several medium configurations in the following section and compared with predictions of analytical methods for either volume and surface scattering when appropriate. The parameters used for the brine inclusions and ice surface are derived from physical observations of temperature, salinity, size distribution, and surface roughness during the CRREL experiments (CRRELEX) [23] and using the brine dielectric constant model of [24].

The boundary of the sea ice medium is modeled either as a flat surface or with a surface roughness typical of first-year sea ice (i.e. sea ice that is less than one year old and has not undergone a melting and refreezing cycle). Scattering is considered both with and without volume scatterers in the sea ice medium to investigate their effects. For the rough surface case, two sets of surface statistics are considered, one more rough than the other. Comparisons are made with the analytical small perturbation method (SPM) for rough surface scattering for the nonvolume scattering case as a validation of the FDTD procedure when appropriate. SPM results when presented are obtained for a three-dimensional (3-D) dielectric rough surface having a dielectric constant equal to that of the background material and excited by an incident plane wave.

Surface profiles were generated following [9] as realizations of a Gaussian random process with a Gaussian correlation function, and are therefore completely characterized by the surface rms height σ and correlation length l parameters. A Gaussian correlation function is commonly used in modeling rough surfaces [8]. However, for sea ice surface roughness, both Gaussian and exponential correlation functions have been proposed [25]. The exact nature of a sea ice surface roughness correlation functions remains unknown.

Due to the small rms heights of the surfaces considered, an additional nonuniform grid was required in the FDTD mesh near the surface in order to capture the surface profile and minimize discretization errors. Tests showed that surface profile discretization errors could become significant at incidence angles larger than 45°, similar to the conclusions of Hastings *et al.* [10]

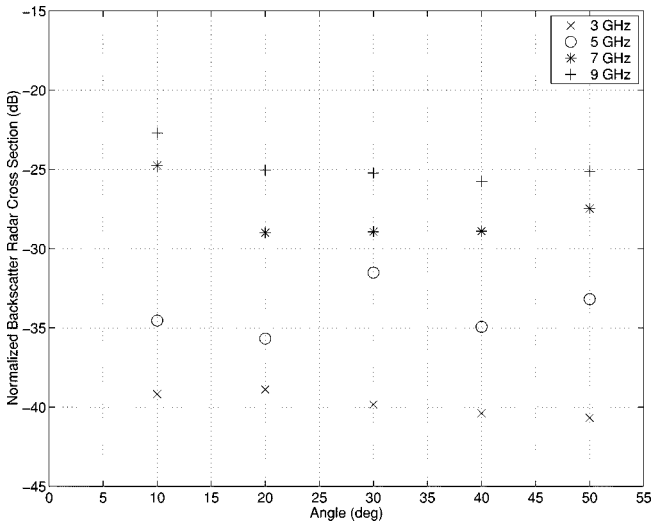

Fig. 3. FDTD incoherent average vv backscattered cross sections versus incidence angle (volume scattering medium with a flat boundary).

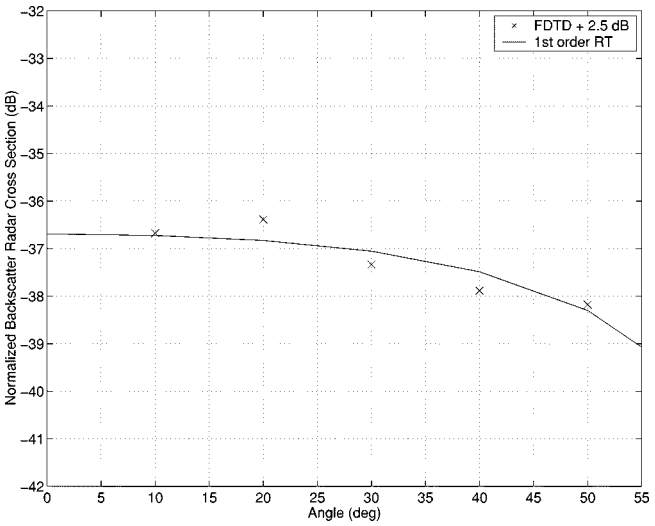

Fig. 4. Comparison of FDTD and first-order iterative RT predictions at 3 GHz for a volume scattering medium with a flat boundary. Note FDTD predictions are increased by 2.5 dB.

for one-dimensional (1-D) PEC surfaces. To avoid these problems, the cell size in the vertical z direction was reduced from 2 mm to 0.5 mm in the region containing the rough surface, allowing a finer resolution of the surface profile in the FDTD mesh. In all cases, the surface profile was terminated two cells away from the PML region (i.e., the roughness inside the PML is set to zero).

A. Case 1: Flat Surface

Initially, volume scattering from an inhomogeneous medium below a flat surface is considered. The ice background relative dielectric constant is $\epsilon = 3.2 - j0.0$, and the spherical brine inclusions have a fractional volume of 10%, a radius of 0.75 mm, and a relative dielectric constant of $50 - j50$. The equivalent fractional volume and dielectric constant for the FDTD cells are 45% and $\epsilon = 5.1 - j0.9/f_{GHz}$, where f_{GHz} is the frequency in GHz. The sea ice layer thickness is 9.5 cm.

Fig. 3 plots incoherent backscattered vv cross sections from 10° to 50° at frequencies of 3, 5, 7, and 9 GHz. The small variation in cross sections with incidence angle (within 5 dB) is a typical characteristic of incoherent volume scattering. Cross sections increase by approximately 15 dB from 3 to 9 GHz. The angular variation at other frequencies between 3 and 9 GHz is similar to that shown in Fig. 3. Some "ripple" can be observed in the numerical results due to the finite number of realizations. Using a larger number of realizations would provide a smoother curve but again was beyond computational limitations.

A test of first-order radiative transfer theory can be performed through comparison with FDTD results. Shin *et al.* [22] give the first-order iterative solution to the radiative transfer (RT) equation for the scattered field from a slab of homogeneous material containing a random distribution of spherical scatterers. The derivation assumes Rayleigh scattering and is valid for the case where scattering from the particles is small. To obtain a clearer comparison, RT predictions are generated for the FDTD approximated, higher fractional volume scatterers, with the spherical scatterer radius for the RT computations defined as $a = 1.24$ mm to produce a sphere with a volume equal to that of the FDTD cell. RT predictions at 3 GHz are found to overestimate FDTD results by approximately 2.5 dB, as shown in Fig. 4, where FDTD cross sections are plotted with a 2.5 dB shift. This discrepancy is possibly due to the independent scattering assumption inherent in the first-order solution, as has been observed by other investigators when using RT to compute volume scattering from snow [7]. The discrepancy is found to increase with frequency as well. Similar trends are observed for smaller fractional volumes [19].

Although questions with regard to the accuracy of a first-order iterative RT solution do not allow a thorough validation of the FDTD approach for this case, the matching of general levels and data trends between theories shows that the numerical model, even with its inherent approximations, is providing reasonable predictions for a volume scattering medium.

B. Case 2: Rough Surface with $\sigma = 0.001$ m, $l = 0.02$ m

Next, a slightly rough dielectric surface with $\epsilon = 3.2 - j0.0$ and surface roughness parameters $\sigma = 0.001$ m and $l = 0.02$ m is considered. Fig. 5 plots the average incoherent vv normalized RCS at 3, 5, 7, and 9 GHz for angles between 10° and 50° backscattered from a surface with no volume scatterers in the lower medium. Also included in Fig. 5 are predictions of the SPM, which are expected to be approximately valid when $k\sigma < 0.3$ and $kl < 3.0$, where k is the electromagnetic wavenumber. Table I lists values of kl and $k\sigma$ corresponding to $f = 3$, 5, 7, and 9 GHz, $l = 0.02$ m and $\sigma = 0.001$ m, and shows that the SPM predictions should be valid for the 3, 5, and 7 GHz frequencies. SPM and FDTD results at these frequencies are within 3 dB except for the 10° point at 3 GHz, which is within 5 dB and possibly influenced more by the finite FDTD source than the larger angles and higher frequencies. The overestimation on average of SPM plane wave predictions by the finite source FDTD results at frequencies above 3 GHz is also as expected, since an angular averaging over the SPM curve would result in a slight increase in cross sections, particularly with the

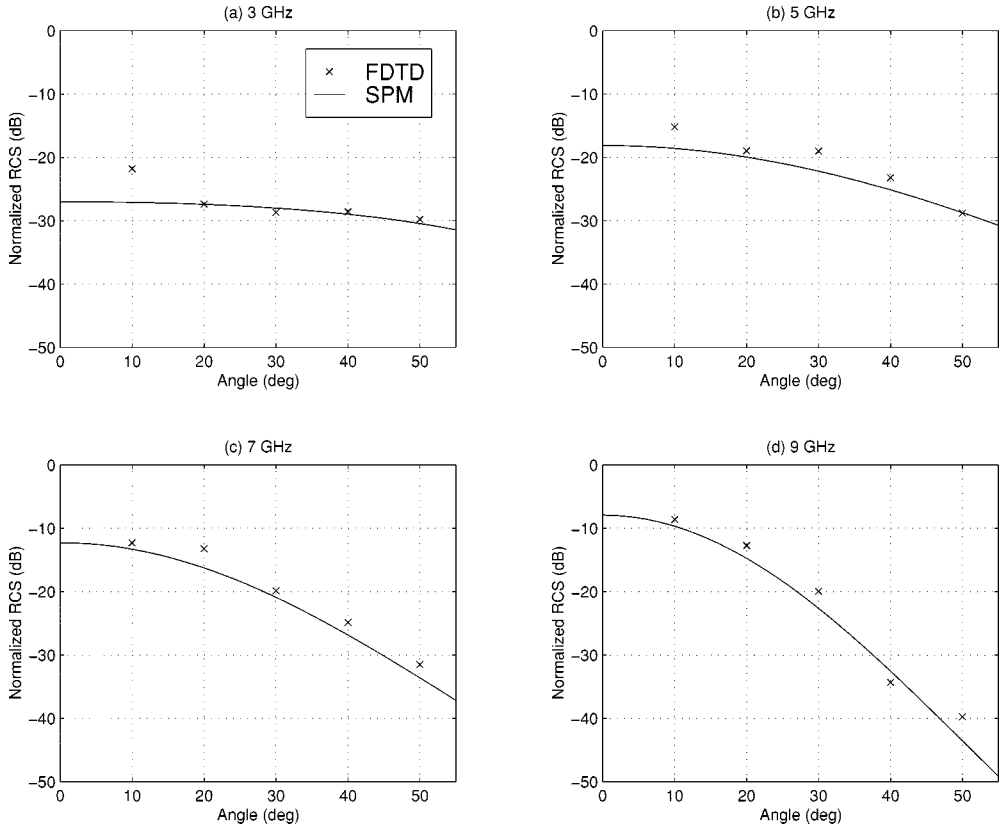

Fig. 5. Comparison of FDTD and SPM incoherent vv average backscattered cross sections versus incidence angle (homogeneous medium with a rough boundary $\sigma = 0.001$ m, $l = 0.02$ m). (a) 3 GHz, (b) 5 GHz, (c) 7 GHz, and (d) 9 GHz.

TABLE I
VALUES OF kl AND $k\sigma$ FOR $l = 0.02$ m AND $\sigma = 0.001$ m

f	3 GHz	5 GHz	7 GHz	9 GHz
kl	1.26	2.09	2.92	3.81
$k\sigma$	0.063	0.105	0.146	0.190

more sloped curves of the higher frequencies. However, the general agreement between the two validates the FDTD nonuniform grid for modeling the effects of surface roughness. Overall trends show rough surface backscattering to be a stronger function of incidence angle than volume scattering as expected, and also to show a strong dependence on frequency.

Fig. 6 compares FDTD average cross sections for the same set of surfaces with and without volume scatterers. Parameters for the inclusions are the same as those for the smooth surface case above, and for each realization, both the surface profile and the brine distribution are varied. The increase in cross sections when including volume scattering is about 2 dB at all incidence angles for 3 and 5 GHz. However, more dramatic increases are observed at 7 and 9 GHz at the larger incidence angles, with the surface-plus-volume case exceeding the surface-only case by more than 10 dB at some angles. Note the point at 50° in the 9 GHz results shows an unrealistic increasing angular trend for a volume scattering medium. Again, the precise values of single points should not be overly examined due to the inherent errors in a Monte Carlo simulation. Overall trends of these curves, however, clearly show that volume scattering can be a significant effect for slightly rough surfaces at large incidence angles.

Fig. 7 compares FDTD results run with both a rough surface profile and volume scatterers to the sum of FDTD results run with a rough surface and no volume scatterers (Fig. 5) and run with a flat surface with volume scatterers (Fig. 3). Cross sections were converted and added in terms of field magnitudes and then converted back to dB. The reasonable agreement (within 2.5 dB) between the numerically calculated surface and volume case and the added surface-only and volume-only results gives some validation to separate consideration of surface and volume effects, as is done in many analytical models.

C. Case 3: Rough Surface with $\sigma = 0.003$ m, $l = 0.02$ m

Fig. 8 compares FDTD average cross sections with and without volume scatterers for rougher surfaces with $\sigma = 0.003$ m. SPM results are also included in the plots, but a multiplication of the $k\sigma$ values in Table I by three (since Table I $k\sigma$ values were computed using $\sigma = 0.001$) shows that SPM predictions should only be approximately valid for the 3 and 5 GHz frequencies. A level of agreement similar to that of Fig. 5 is observed when comparing FDTD and SPM results at these frequencies. A general increase in surface-only backscattered cross sections is observed for this rougher surface case when compared to Fig. 5, particularly at higher frequencies and larger incidence angles. The addition of volume scatterers is observed to have a less significant effect than in Fig. 6 due to the increased surface contribution at larger incidence angles,

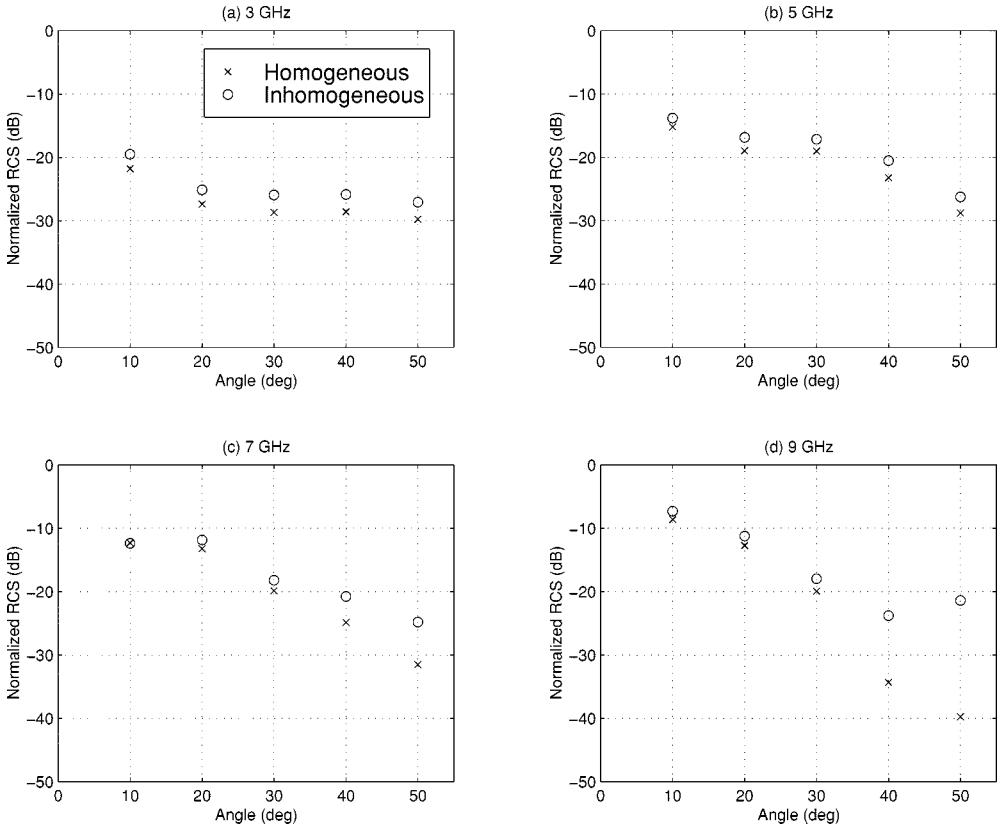

Fig. 6. Comparison of FDTD incoherent vv average backscattered cross sections versus incidence angle for homogeneous and inhomogeneous media with a rough boundary $\sigma = 0.001$ m, $l = 0.02$ m. (a) 3 GHz, (b) 5 GHz, (c) 7 GHz, and (d) 9 GHz.

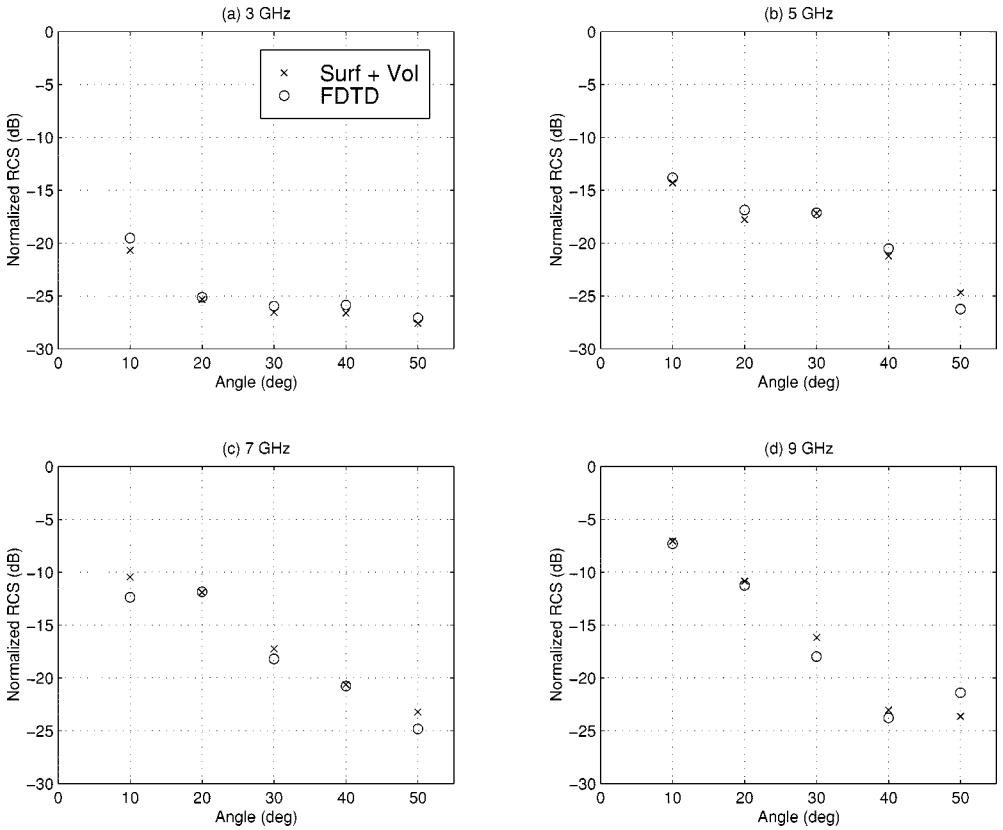

Fig. 7. FDTD incoherent vv average backscattered cross sections versus incidence angle for an inhomogeneous medium with a rough boundary $\sigma = 0.001$ m, $l = 0.02$ m. Comparison of FDTD surface and volume results with the sum of FDTD results with volume scattering only and with surface scattering only. (a) 3 GHz, (b) 5 GHz, (c) 7 GHz, and (d) 9 GHz.

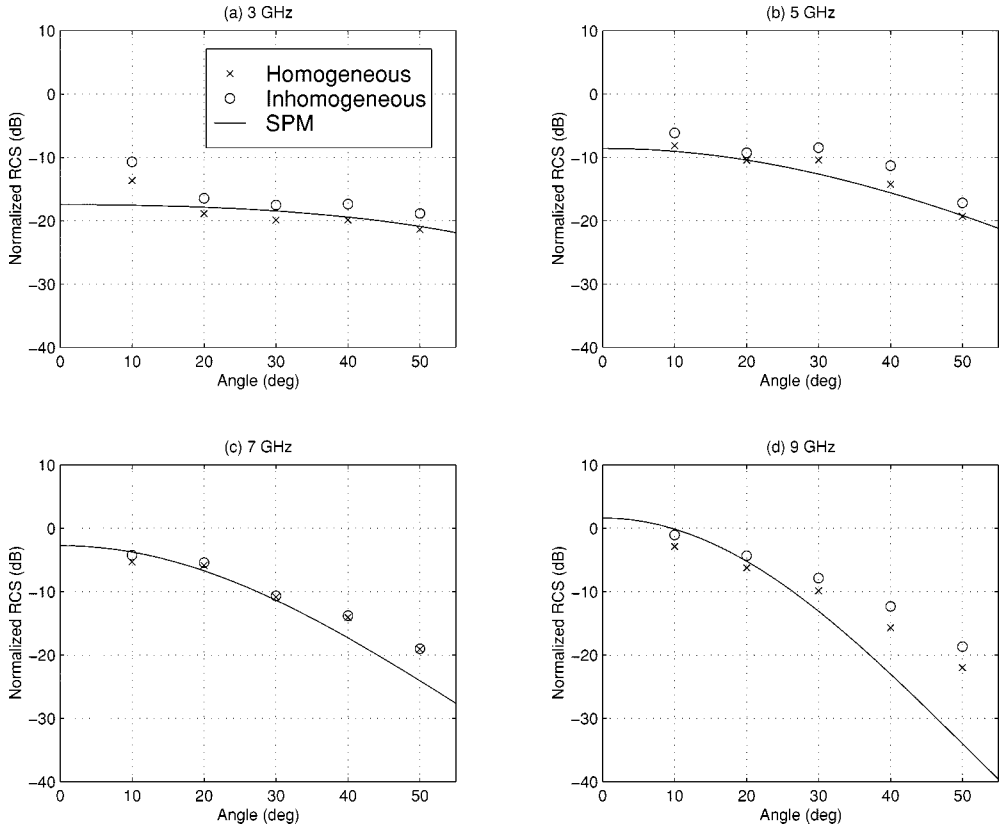

Fig. 8. Comparison of FDTD incoherent vv average backscattered cross sections versus incidence angle for homogeneous and inhomogeneous media with a rough boundary $\sigma = 0.003$ m, $l = 0.02$ m. SPM predictions for surface-only scattering are also included. (a) 3 GHz, (b) 5 GHz, (c) 7 GHz, and (d) 9 GHz.

and differences are within the expected level of error of the simulation. Thus, it appears that surface scattering is the dominant effect for this set of medium parameters. Fig. 9 shows that the addition of surface-only and volume-only predictions is again approximately valid for this case, matching FDTD surface and volume predictions within 3 dB.

IV. Comparison with CRREL Measurements

Although the approximations of the numerical model and a lack of complete ground truth data make a direct comparison with measured data difficult, a preliminary comparison is made in this section to compare trends in the modeled and measured data. Two cases are considered: bare ice with a smooth surface and pancake ice with a rough surface.

A. Smooth Bare Ice

Fig. 10 compares FDTD predictions for the backscattered normalized RCS in the flat surface, volume scattering case (Fig. 3) with measurements taken from a very smooth bare ice surface using a plane wave antenna [26] during CRREL in January of 1994. Reference [23] specifies the measured rms roughness for the bare ice section to be less than 0.001 m, so that volume scattering is likely to be the dominant effect at larger incidence angles, and the flat surface FDTD model is reasonable for comparison. Measured data is plotted only up to 30° because data at larger angles could not be recovered due to the dynamic range of the radar system and was interpolated to the 7 and 9 GHz frequencies shown from data samples at 6.5, 7.5, 8.5, and 9.5 GHz. This interpolation is not expected to contribute significant error because the frequency swept data was relatively smooth in this range of frequencies. Although significant differences in cross section levels are observed, particularly at 7 GHz, measurement and modeled data show similar trends in their variation with incidence angle. The slow falloff in 9 GHz measured cross sections for incidence angles beyond 10° matches FDTD predictions for a volume scattering only medium well, again demonstrating the importance of volume scattering for a very smooth surface case, even at higher frequencies.

B. Pancake Sea Ice

Measurements taken from a pancake ice sample during CRREL '95 [27] are plotted in Fig. 11 and compared with results from the FDTD model with $\sigma = 0.003$ m, $l = 0.02$ m and inclusions. Reference [23] specifies the measured rms roughness for this case as 0.0019 m, somewhat less than the FDTD surfaces, and other physical characteristics of pancake ice including a smaller thickness and higher salinity content are not included in the FDTD model. Again, significant discrepancies between FDTD and measured results are observed. However, the agreement in general trends shows that the dominant surface scattering effect can probably explain results for the pancake ice at angles from 5° to 50°.

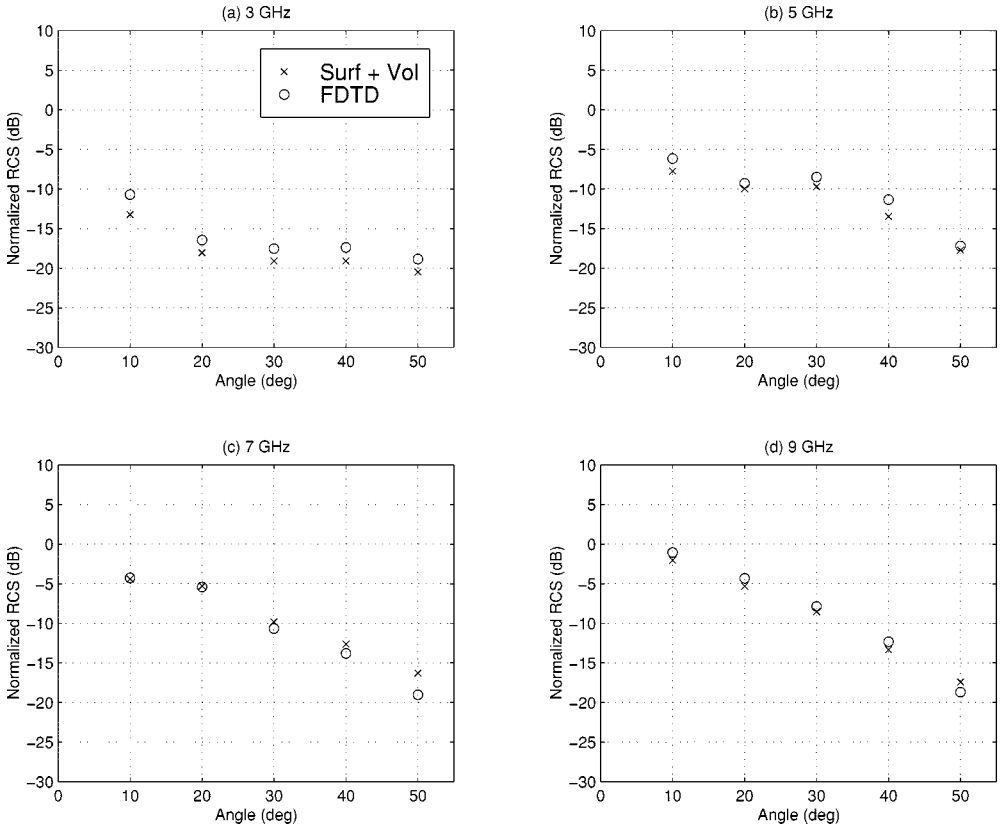

Fig. 9. FDTD incoherent vv average backscattered cross sections versus incidence angle for an inhomogeneous medium with a rough boundary $\sigma = 0.003$ m, $l = 0.02$ m. Comparison of FDTD surface and volume results with the sum of FDTD results with volume scattering only and with surface scattering only. (a) 3 GHz, (b) 5 GHz, (c) 7 GHz, and (d) 9 GHz.

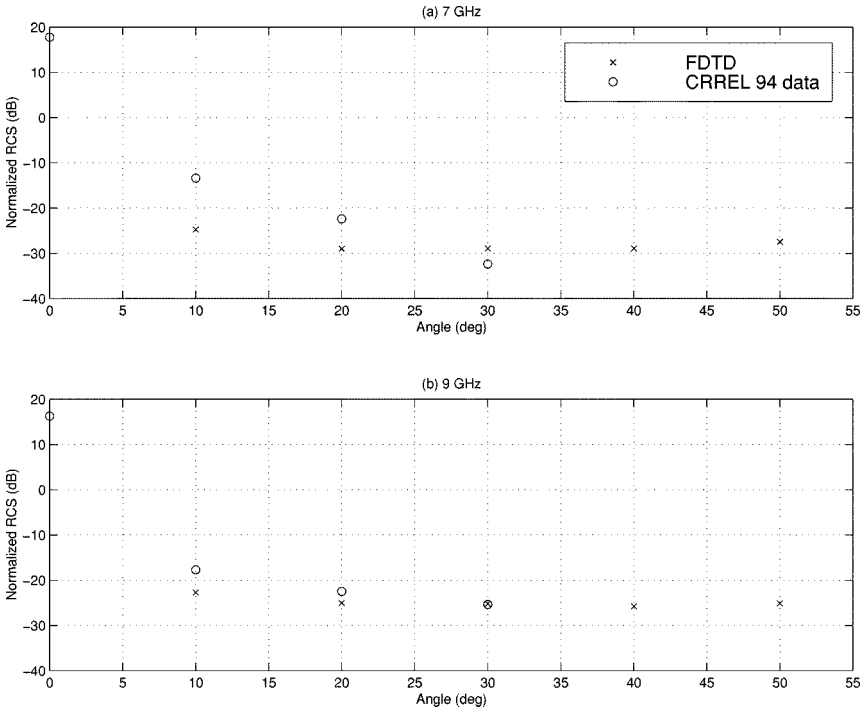

Fig. 10. Comparison of FDTD with CRREL '94 measurements for bare ice. (a) 7 GHz and (b) 9 GHz.

V. Conclusion

A numerical model for electromagnetic scattering from sea ice was developed and validated. The model was used to predict the backscattered RCS from sea ice models with smooth and slightly rough surfaces. Although the computational intensity of a Monte Carlo simulation limited the number of realizations obtained and necessitated approximations in modeling of

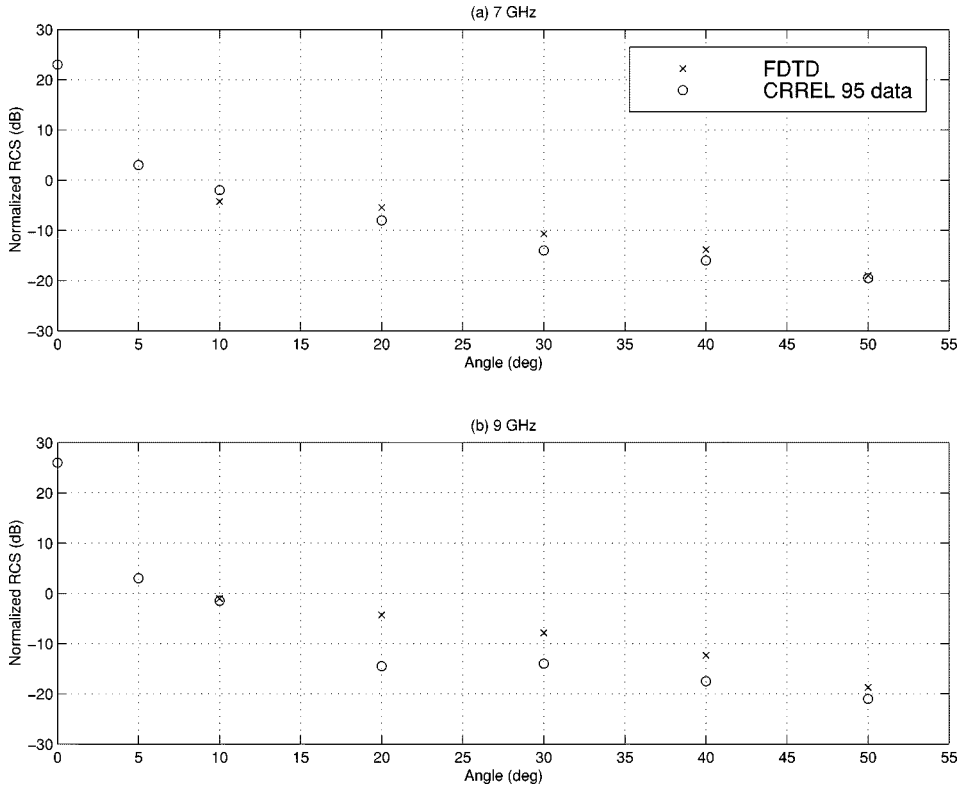

Fig. 11. Comparison of FDTD with CRREL '95 measurements for pancake ice. (a) 7 GHz and (b) 9 GHz.

the sea ice medium, comparison of FDTD results with analytical approximate theories in appropriate cases showed that predicted cross sections should be accurate to within approximately 3 dB. Studies of the relative effects of volume and surface scattering showed that both can contribute to observed cross sections, with volume scattering primarily observable with smooth surfaces at larger incidence angles. Comparisons of numerical results including both surface and volume scattering with a sum of surface-only and volume-only contributions showed separate consideration of these effects to be reasonably accurate for the medium parameters considered.

The 3-D numerical model presented provides an additional tool for further understanding of the sources of scattering in sea ice and could be applied in the development of inverse scattering models or to study volume and surface scattering from other geophysical media. Although the model remains computationally intensive, the ability to avoid electromagnetic approximations in the solution makes it a useful tool when medium parameters lie outside the range of analytical models.

ACKNOWLEDGMENT

The authors would like to thank the Maui High Performance Computing Center for the use of the IBM SP/2.

REFERENCES

[1] F. D. Carsey, Microwave Remote Sensing of Sea Ice, Geophysical Monograph 68, American Geophysical Union, 1992.
[2] A. Ishimaru, *Wave Propagation and Scattering in Random Media*. New York: Academic, 1978.
[3] L. Tsang, J. Kong, and R. Shin, *Theory of Microwave Remote Sensing*. New York: Wiley, 1985.
[4] P. Beckmann and A. Spizzichino, *The Scattering of Electromagnetic Waves from Rough Surfaces*. New York: Pergamon, 1963.
[5] S. Rice, "Reflection of electromagnetic waves from slightly rough surfaces," *Commun. Pure Appl. Math.*, vol. 4, pp. 351–378, 1951.
[6] A. K. Fung, *Microwave Scattering and Emission Models and Their Applications*. Boston, MA: Artech House, 1994.
[7] L. M. Zurk, L. Tsang, and D. P. Winebrenner, "Scattering properties of dense media from Monte Carlo simulations with application to active remote sensing of snow," *Radio Sci.*, vol. 31, pp. 803–819, July–August 1996.
[8] A. K. Fung, M. R. Shah, and S. Tjuatja, "Numerical simulation of scattering from three-dimensional randomly rough surfaces," *IEEE Trans. Geosci. Remote Sensing*, vol. 32, Sept. 1994.
[9] J. T. Johnson, "Application of numerical models for rough surface scattering,", Ph.D. dissertation, Mass. Inst. Technol., Cambridge, Feb. 1996.
[10] F. D. Hastings, J. B. Schneider, and S. L. Broschat, "A Monte Carlo FDTD technique for rough surface scattering," *IEEE Trans. Antennas Propagat.*, vol. 43, Nov. 1995.
[11] K. S. Yee, "Numerical solution of initial boundary value problems involving Maxwell's equations in isotropic media," *IEEE Trans. Antennas Propagat.*, vol. AP-14, pp. 302–307, May 1966.
[12] C. H. Chan, S. H. Lou, L. Tsang, and J. A. Kong, "Electromagnetic scattering of waves by rough surfaces: A finite-difference time-domain approach," *Microw. Opt. Technol. Lett.*, vol. 4, no. 9, pp. 355–359, 1991.
[13] K. Demarest, R. Plumb, and Z. Huang, "FDTD modeling of scatterers in stratified media," *IEEE Trans. Antennas Propagat.*, vol. 43, pp. 1164–1168, 1995.
[14] K. Demarest, Z. Huang, and R. Plumb, "An FDTD near- to far-zone transformation for scatterers buried in stratified grounds," *IEEE Trans. Antennas Propagat.*, vol. 44, pp. 1150–1157, Aug. 1996.
[15] A. Taflove, *Advances in Computational Electrodynamics: The Finite-Difference Time-Domain Method*. Boston, MA: Artech House, 1998.
[16] J. P. Berenger, "A perfectly matched layer for the absorption of electromagnetic waves," *J. Comput. Phys.*, vol. 114, pp. 185–200, Oct. 1994.
[17] W. C. Chew and W. H. Weedon, "A 3-D perfectly matched medium from modified Maxwell's equations with stretched coordinates," *Microw. Opt. Technol. Lett.*, vol. 7, pp. 599–604, Sept. 1994.
[18] A. Bahr, A. Lauer, and I. Wolff, "Applications of the PML absorbing boundary condition to the FDTD analysis of microwave circuits," *MTT-Symp. Dig.*, pp. 27–30, 1995.

[19] E. M. Nassar, "Numerical and experimental studies of electromagnetic scattering from sea ice," Ph.D. dissertation, The Ohio State Univ., Columbus, 1997.
[20] C. A. Balanis, *Advanced Engineering Electromagnetics*. New York: Wiley, 1989, ch. 6.
[21] F. Ulaby, R. Moore, and A. Fung, *Microwave Remote Sensing: Active and Passive*. Reading: Addison-Wesley, 1962, vol. 3.
[22] R. T. Shin and J. A. Kong, "Radiative transfer theory for active remote sensing of a homogeneous layer containing spherical scatterers," *J. Appl. Phys.*, vol. 52, June 1981.
[23] BPRC Tech. Note 94-02, Byrd Polar Res. Center, The Ohio State Univ., Columbus, July 21, 1994.
[24] A. Stogryn and C. J. Desargeant, "The dielectric properties of brine in sea ice at microwave frequencies," *IEEE Trans. Antennas Propagat.*, vol. AP-33, pp. 523–523, May 1985.
[25] I. Zabel, K. Jezek, S. P. Gogineni, L. Lockhart, and R. Hosseinmostafa, "Time dependent model for radar backscatter from sea ice," in *Proc. Workshop on Modeling the Electromagnetic Properties of Sea Ice*, West Lebanon, NH, Jan. 15–16, 1994.
[26] S. Gogineni, K. Jezek, L. Peters, J. Young, S. Beaven, and E. Nassar, "Application of plane waves for accurate measurement of microwave scattering from geophysical surfaces," *IEEE Trans. Geosci. Remote Sensing*, vol. 33, May 1995.
[27] L. Peters, Jr., K. Jezek, and P. Gogineni, "Report to CRREL sea ice studies," , to be published.

Elias M. Nassar received the B.E. degree in electrical engineering (with distinction) from the American University, Beirut, Lebanon, in 1990, and the M.S. and Ph.D. degrees in electrical engineering from The Ohio State University (OSU), Columbus, in 1992 and 1997, respectively.

From 1990 to 1997, he was a Graduate Research Assistant with the ElectroScience Laboratory, OSU, where he worked on numerical modeling and testing of antennas for ground penetrating radar and remote sensing of sea ice. In 1997, he was a Graduate Teaching Assistant in the Electrical Engineering Department at OSU, where he taught laboratory courses. In 1998, he joined the faculty of the Electrical and Computer Engineering Department, Notre Dame University, Lebanon, as an Assistant Professor. His current research interests include the use of numerical methods in electromagnetics to model antennas for mobile communications and radar remote sensing, and developing novel methods in engineering education.

Joel T. Johnson (M'96) received the B.E.E. degree from the Georgia Institute of Technology, Atlanta, in 1991, and the S.M. and Ph.D. degrees from the Massachusetts Institute of Technology, Cambridge, in 1993 and 1996, respectively.

He is currently an Assistant Professor in the Department of Electrical Engineering and ElectroScience Laboratory, The Ohio State University, Columbus. His research interests are in the areas of microwave remote sensing, propagation, and electromagnetic wave theory.

Dr. Johnson is an Associate Member of Commissions B and F of the International Union of Radio Science (URSI), and a member of Tau Beta Pi, Eta Kappa Nu, and Phi Kappa Phi. He received the 1993 Best Paper Award from the IEEE Geoscience and Remote Sensing Society and was named an Office of Naval Research Young Investigator, National Science Foundation Career awardee, and PECASE award recipient in 1997.

Robert Lee received the B.S.E.E. degree from Lehigh University, Bethlehem, PA, in 1983 and the M.S.E.E. and Ph.D. degrees from the University of Arizona, Tucson, in 1988 and 1990, respectively.

From 1983 to 1984, he worked for Microwave Semiconductor Corporation, Somerset, NJ, as a Microwave Engineer. From 1984 to 1986, he was a Member of Technical Staff, Hughes Aircraft Company, Tucson. From 1986 to 1990, he was a Research Assistant with the University of Arizona. In addition, during the summers of 1987 through 1989, he worked at Sandia National Laboratories, Albuquerque, NM. Since 1990, he has been with The Ohio State University, Columbus, where he is currently an Associate Professor. His major research interests are in the analysis and development of finite methods for electromagnetics.

Dr. Lee is a Member of the International Union of Radio Science (URSI).